Construction and Building Materials 322 (2022) 126491

Contents lists available at ScienceDirect

Construction and Building Materials

journal homepage: www.elsevier.com/locate/conbuildmat

Eco-friendly treatment of recycled concrete fines as supplementary cementitious materials

Liang Wang [a,b,c], Jialai Wang [b,*], Hao Wang [a], Yi Fang [b], Wenfeng Shen [a], Peiyuan Chen [a], Ying Xu [a]

[a] School of Civil Engineering and Architecture, Anhui University of Science and Technology, Huainan, Anhui 232001, PR China
[b] Department of Civil, Construction, and Environmental Engineering, The University of Alabama, Tuscaloosa, AL 35487, USA
[c] Huaibei Mining Co. Ltd., Huaibei, Anhui 235000, PR China

ARTICLE INFO

Keywords:
Recycled concrete fine
Tannic acid
Supplementary cementitious materials
Compressive strength
Corrosion resistance
Nanoindentation

ABSTRACT

Demolished or waste concretes can be crushed into particles with appropriate sizes to be used as coarse or fine aggregates in new concretes. This recycling process also produces 5% to 20% small particles with size less than 0.15 mm. which can be recycled as the recycled concrete fines (RCFs). Besides low-end applications and landfilling, few appropriate applications have been found for RCF. This study develops an eco-friendly treatment to turn these underutilized RCFs into supplementary cementitious materials (SEM) for new concretes. Without any treatment, RCFs can significantly reduce the strength and durability of the produced concrete due to their low pozzolanic activity and high porosity. This study exploits a plant-based compound, tannic acid (TA) to treat RCFs so they can be used in new concrete to partially replace Portland cement without reducing the performance of the concrete. This is done by a simple two-step mixing process. In the first step, RCF particles are mixed with a low-concentrated TA solution for about one hour to allow for potential reaction between the TA and the RCF particles. In step II, the slurry produced by step I is mixed with cement and aggregate to make concrete. Reaction between the TA and the RCF particles can produce submicron particles deposited on the surface of the RCF particles. Those particles not only fill the pores of the RCF particles, but also provide the nucleation sites for the hydration of the cement. This promotes the hydration of the cement and densifies the microstructure of the hardened paste. As a result, multiple benefits can be induced by the proposed TA treatment. Experimental results show that up to 26% increment in compressive strength of the mortar has been achieved by the proposed treatment. More importantly, the risk of cracking in the early age of the mortar is reduced and the corrosion life of the reinforcing bar is greatly enhanced.

1. Introduction

Construction and demolition (C&D) wastes are the largest waste streams in many countries all over the world. The ever-increasing production of C&D wastes not only occupy enormous space for landfill sites, but also result in a series of environmental issues such as water, atmospheric and soil pollution [1,2]. Concrete waste accounts for approximately 65% of C&D waste [3]. It is a common approach to crush the concrete wastes into particles with appropriate size to be used as coarse or fine aggregates in new concretes [1,4,5]. However, this process can generate 5% to 20% fine particles with size less than 0.15 mm, which cannot be used as aggregates in new concrete [6,7]. The main components of these fines particles are hydrated calcium silicate, unhydrated cement particles, calcium hydroxide (CH) and fines of aggregates [7,8]. Among them, the unhydrated cement particles and CH can further hydrate to produce gel products or seed the hydration of cement [9]. Therefore, these particles have been recycled as a supplementary cementitious material (SCM) for concrete or mortar [10,11] to partially replace ordinary Portland cement (OPC), leading to reduction of the carbon footprint of produced concrete. However, the reactivity of these recycled concrete fines (RCFs) is much lower than that of OPC. As a result, the mechanical strength and durability of the produced concrete with RCF can be significantly reduced [12,13]. The workability of concrete can also be reduced since more mixing water is absorbed by the RCF during the mixing process [14]. Duan et al. [15] observed that using RCF in a self-consolidated concrete led to agglomeration of particles in

* Corresponding author.
E-mail address: Jwang@eng.ua.edu (J. Wang).

https://doi.org/10.1016/j.conbuildmat.2022.126491
Received 17 September 2021; Received in revised form 19 November 2021; Accepted 14 January 2022
Available online 22 January 2022

the cement matrix, which attributes to the poor workability, mechanical strength and durability of concrete with RCF.

Many efforts have been made to improve the reactivity of RCFs, including thermal, physical and chemical excitations. In thermal excitation, RCFs are heated to a high temperature to dehydrate the hydration products so that more active components can be produced [9,16]. In physical excitation, RCFs are ground into finer particles by centrifugal ball milling. Mechanical force can distort the tetrahedral structure of α-SiO_2 and transform it into amorphous SiO_2 [17]. Meanwhile, more Ca$(OH)_2$ and unhydrated cement particles can be released during the ball milling. The ability of RCFs to participate in cement hydration is improved after physical excitation [18]. Li et al. [19] showed that the compressive strength of mortar with ground RFC as SCM increases with the fineness of RCF. In chemical excitation, acids or alkali salts are used to improve the reactivity RCFs in cement. For example, Prošek et al. [20] used lime, fly ash and slag as activators to improve the reaction activity of RCFs. The compressive and flexural strengths of the concrete made with activated RCFs are higher than that of the concrete made with untreated RCP. Recently, carbonation with CO_2 has emerged as a promising chemical treatment for RCFs [21–23]. Reaction between CO_2 and hydration products in RFCs produces calcium carbonate particles acting as a fine filler and silica-alumina gel acting as a pozzolanic material with high reactivity [22]. This method not only improves the performance of the produced concrete, but also permanently store some CO_2 in the concrete. Shen et al. [23] showed that a two-step wet carbonation process can absorb 0.27 g CO_2 per 1 g RCF, and the microstructure was significantly improved by the carbonation.

In this study, an eco-friendly chemical treatment for RCFs is proposed to enhance the performance of cement mortars made with treated RCFs as SCM. This method can be simply carried out by a two-step mixing process. In the first step, RCF is mixed with a low-concentrated TA solution for about one hour to allow for reaction between TA and RCF. The resulting slurry from step I is mixed with cement and aggregate to make concrete in Step II. TA is a water solvable plant polyphenol, and is the world's third largest class of plant product after cellulose and lignin[24]. It can be extracted from plants, microorganisms [25], or decomposing organic matters in water [26]. As a result, TA can be obtained at very low cost [27,28]. TA usually can be written as $C_{76}H_{52}O_{46}$ with a center glucose molecule and five hydroxyl moieties esterified with two gallic acids (3,4,5-trihydroxybenzoic acid) molecules (Fig. 1). Due to the presence of benzene rings and hydroxyl groups, TA is easy to form hydrogen bonds, electrostatic, hydrophobic and π-π stacking interactions with many molecules or functional groups [29]. One of the distinctive features of this material is its ability to adhere strongly to the surface of diverse surfaces through covalent interactions and non-covalent interactions [28]. Particularly, the pyrogallol group in TA molecule has the ability to capture calcium ion in aqueous solution, which contributes to the local supersaturating of calcium ion to induce the local mineralization [30,31]. In addition, TA can coordinate with Al^{3+}, Fe^{3+} and other metal ions to form TA-metal network structure [32,33]. Therefore, TA has been successfully applied in the fields of adsorption and antibacterial materials [34,35], nano and micro material [36], capsule [37], film and coating [32,38], biological adhesive [39], hydrogel [40], and nanocomposite [41].

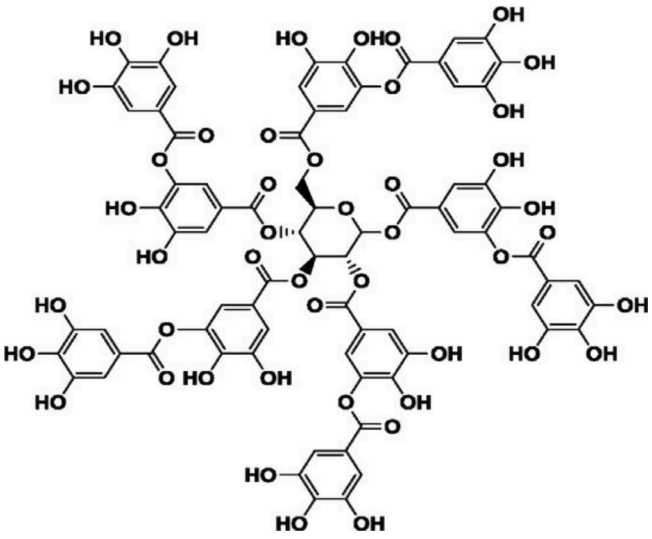

Fig. 1. Tannic acid.

Inspired by many successes of TA, we exploit TA to enhancing the binding capacity of RCFs through the two-step mixing. Reaction between TA and hydration products in RCF particles in Step I can produce small particles which can fill the pores of RCF particles and deposit on the surface of RCF particles to seed the hydration of the cement. Moreover, the excellent binding ability of TA's functional groups coated on the surface of RCF particles can improve the bonding with the hydration products of OPC, leading to improved strength and durability of the produced concrete/mortar with the treated RCF as SCM.

2. Materials and methods

2.1. Materials

OPC is used as binder in this study. RCF is the crushed waste concrete with particle size less than 165 μm collected from Huainan Construction Quality Supervision and Inspection Center, Anhui, China. The chemical compositions of the RCF and OPC are shown in Table 1. Their particle size distributions were determined by a laser diffraction technique using a Mastersizer 2000, as shown in Fig. 2. The median particle size (d_{50}) of the RCF and OPC are 5.0 μm and 14.5 μm, respectively. River sand with fineness modulus of 2.56 and apparent density of 2550 kg/m^3 is used as fine aggregate. Analytically pure TA was purchased from a local supplier. Five different concentrations of TA solution (0.1%, 0.3%, 0.5%, 0.75%, and 1%) were prepared to treat the RCF.

2.2. Characterization of TA treated RCFs

The dried RCF sample was first immersed in TA solution for 60 min. Then, the solid particles were filtered from TA solution and dried in an electric blast drying oven at temperature of 80 °C for 24 h to remove the absorbed water. X-ray diffraction (XRD) and Fourier transform infrared spectrometer (FTIR) analysis were carried out to probe any mineralogical change of the RCF induced by the proposed treatment. Scanning electron microscopy (SEM) analysis was conducted to examine the surface microstructure change of the RCF particles induced by the TA treatment. To do this, RCF samples were coated with a thin layer of gold before the observation. Brunauer Emmett-Teller (BET) was used to examine the change on pore size distribution of RCF samples.

2.3. Manufacture and characterization of mortar specimens with RCF as SCM

2.3.1. Mortar specimen preparation

The water to binder (w/b) in mass was chosen as 0.5 for all mortar mixes in this study. The mix proportions of all mortar are shown in Table 2. The RCF was used to replace cement at 5%, 10%, 15% and 20%. To make these mortars using the proposed two-step mixing method, the RCF was first mixed with TA solution for 60 min. The resulting slurry was them mixed with cement and sand which were homogenized in a mechanical mixing pot for 2 min. After stirring for 2 min, the fresh mortar was cast into 50 mm cubic molds and vibrated on a vibration table for 30 s to remove air bubble in the mortar. The produced fresh mortar specimens were cured in a curing room with temperature of 23 ± 2 °C and relative humidity no less than 95%. After 24 h, the hardened specimens were demolded and further cured for a specific period.

Table 1
Chemical composition of the RCF and OPC.

Materials	Chemical composition/wt.% (XRF)							
	SiO_2	Al_2O_3	CaO	MgO	Fe_2O_3	TiO_2	K_2O	Others
RCF	33.4	8.4	44.9	5.4	1.0	0.6	1.7	4.6
OPC	26.5	18.2	43.7	4.9	3.9	1.0	0.8	1.0

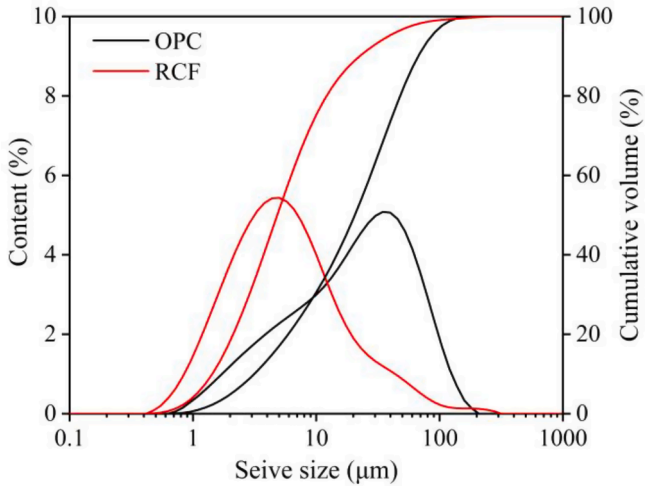

Fig. 2. Particle sizes distribution of RCF and OPC.

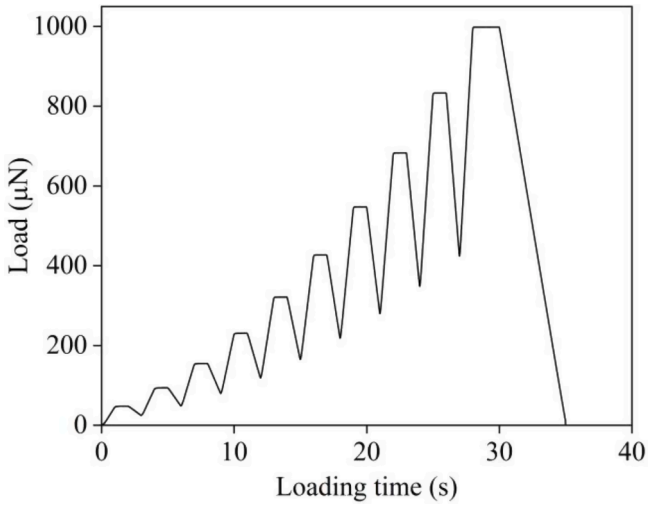

Fig. 3. Loading function of nanoindentation test.

Table 2
Mix proportions (kg/m^3) materials for mortar manufacture.

Notation	Cement	RCF	Water	Sand
Control	547	0	275	1430
5%RCF	519.7	27.3	275	1430
10%RCF	492.3	54.7	275	1430
15%RCF	464.9	82.1	275	1430
20%RCF	437.6	109.4	275	1430

2.3.2. Characterization of the mortar specimen with RCFs

The compressive strengths of mortar specimens were measured at 3d, 7d and 28d according to ASTM C109 [42]. The average value of three duplicated specimens were used as the measured compressive strength.

Isothermal calorimetry was conducted to examine the effect of the proposed treatment on the hydration of the cement according to ASTM C1702-17 [43]. The heat released by the cement hydration was recorded for the first 70 h by a TAM-AIR (Thermometric AB, Sweden). After calorimetry testing, the paste samples were cured in sealed conditions for 3d and 28d. Then these paste samples were pulverized and ground into fine powders. #100 mesh (0.15 mm) was used to sieve the fine powders for XRD analysis to examine the effect of TA treatment on hydration products.

Mercury intrusion porosimetry (MIP) was used to examine the pore structures of the mortar samples by a Micromeritics AutoPore 9500. The crushed samples after the compressive strength test at age of 28d were used in MIP analysis.

Effect of the proposed treatment on micromechanical properties of cement was examined by nanoindentation testing using a TI 950 TriboIndenter nanoindenter with a pyramid shaped diamond Berkovich indenter tip. Load control mode was used during the testing, in which the maximum load of 1000μN was attained by the linear loading steps at the tenth cycle, as shown in Fig. 3. The loading time, holding time and unloading time were all one second for the first nine loading cycles to eliminate effect of the creep and surface roughness [44]. At the last cycle of loading, the maximum load (1000μN) was hold for 2 s and unloaded linearly to zero for 5 s. The stiffness was measured by the last unloading segment of each indent. The Poisson ratio was assumed as 0.2 for the cement paste. The elastic modulus of each test was calculated according to the Oliver and Pharr method [45]. The test was conducted on a 20 × 20 array with 5 μm. Elastic modulus of the selected testing area was analyzed spatially using a mapping method [46]. Statistical deconvolution techniques are used for multiphase heterogeneous and heterogeneous materials, such as cement paste, to determine volume fractions and average mechanical properties of each phase. The deconvolution process was performed by using Gauss Mixture Model (GMM). The indents on calcium silicate hydrate (C-S-H) phases was recognized by the elastic modulus smaller than the C-S-H particle stiffness (E ≤ 60 GPa) at the Poisson's ratio equal to 0.2 [47]. Four phases of hydration products (excluding anhydrous clinker minerals) can be identified based on deconvolution results, which are low-density C-S-H (LD), high-density C-S-H (HD), ultra-high density C-S-H (UHD) and portlandite (CH) [48,49].

The packing density of each C-S-H phase was calculated by the following equation [47,50]:

$$\eta_i = 0.5(M_i/m_s + 1), \quad (1)$$

where, η_i is the packing density on the indent area; M_i is the indentation modulus of each point; m_s is the indentation modulus of non-porous solid material. For C-S-H solid, the m_s is fixed to 62.5GPa, which is equal to 60 MPa of elastic modulus, according to Allen [47].

The early-age cracking is critical to the long-term durability of concretes/mortars [51,52]. Therefore, the effect of the proposed treatment on early-age cracking of the mortars was examined following Chinese standard [53]. To this end, the fresh mortar was cast into a mold with a size of 800 mm × 600 mm × 100 mm. The produced specimen was immediately subjected to the testing environment at room temperature of 20 °C ± 2 °C with relative humidity of 60% ± 5%. A fan was used to provide a wind speed of (5 ± 0.5) m/s to accelerate the emerging of cracks on the surface of the specimen. After 24 h, lengths and widths of the cracks were measured using a steel ruler and a microscope magnifier, respectively. The average area of cracks, number of cracks per unit area and crack area per unit area are three parameters to

characterize the cracking behavior of the mortar specimen. Those three parameters are calculated by the following equations,

$$a = \frac{1}{2N}\sum_{i=1}^{N}(W_i \times L_i), \tag{2}$$

$$b = N/A, \tag{3}$$

$$c = a \times b, \tag{4}$$

where, a is the average area of the cracks, N is the number of the cracks, W_i is the maximum width of each crack, L_i is the length of crack i, b is the number of the cracks per unit area, A is the area of the top surface of the specimen, c is the area of the cracks per unit area.

The effect of the proposed treatment on corrosion performance of the produced mortar was examined by a rapid corrosion testing technique. The schematic representation of this testing set-up is shown in Fig. 4(a) and the real testing system is presented in Fig. 4(b). In this testing, a reinforced cement mortar cylinder with size of 100 mm × 200 mm was made and cured in a curing room with temperature of 23 °C ± 2 °C and relative humidity no less than 95% for 28d. Then the specimen was

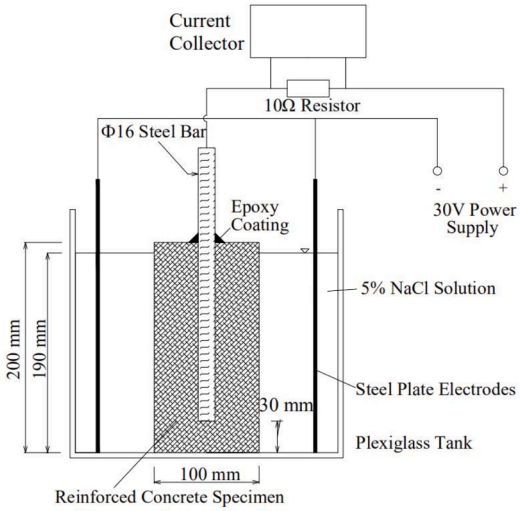

(a) Schematic representation of set-up for the accelerated corrosion test [54]

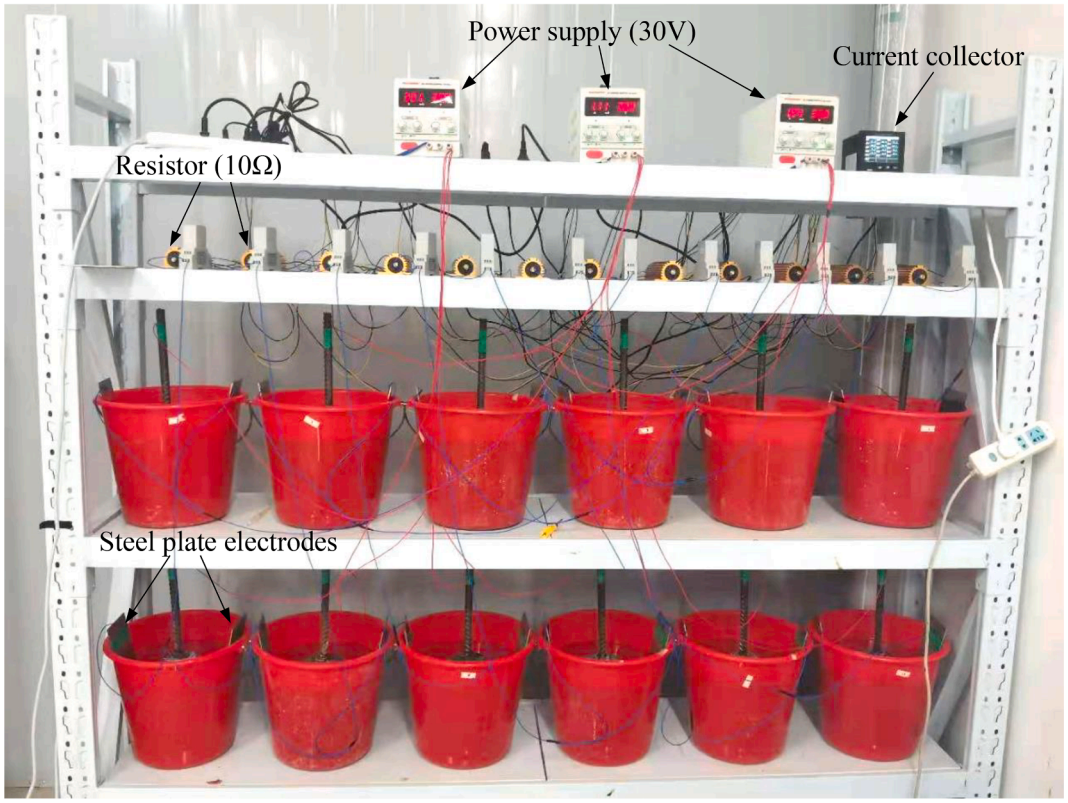

(b) Accelerated corrosion testing set-up

Fig. 4. Accelerated corrosion test set-up for reinforcement bar embedded in cement mortar [54].

immersed in a 5% sodium chloride (NaCl) solution with only 10 mm of the cylinder is above the solution. The corrosion test was conducted at the age of 28d. A 30 V DC power source was connected to the steel bar (anode) and the stainless steel plates (cathode) placed near the specimen in NaCl solution (electrolyte) to initiate a fast corrosion process. Current variation with time was recorded by a data logger. Cccurrence of through crack(s) in the specimen can be identified by an abrupt rise of the current.

3. Results and discussions

3.1. Characterization of RCF

In this section, "Control" refers to the untreated RCF sample; 0.1% TA, 0.3%TA, 0.5%TA and 1%TA refer to the RCF samples treated by 0.1%, 0.3%, 0.5% and 1% TA solution, respectively.

3.1.1. XRD

XRD patterns of the untreated and TA-treated RCF samples are shown in Fig. 5. The main minerals of the untreated RCF sample are quartz, calcium hydroxide (CH), calcite and dolomite. The quartz and dolomite come from fine sand and gravel particles, respectively, which were produced during the crushing process of the waste concrete. CH is the cement hydration product of waste concrete. The existence of calcite indicates that some CH in the waste concrete has been carbonized. The major hydration product, C-S-H is not shown in XRD results since it is mainly amorphous. After the TA treatment, the intensities of peaks of CH at $2\theta = 18^{\circ}$ and 60° are reduced since the chemical reaction occurs between CH and TA solution, consuming some CH by the TA solution. However, no new mineral formation was detected by XRD in RCF samples treated with 0.5% TA and 1%TA. Therefore, FTIR analysis was conducted to examine potential complex formed by the reaction between TA and RCF samples.

3.1.2. FTIR

The results of FTIR spectra of the untreated RCF sample (Control) and the treated samples are shown in Fig. 6. As a comparison, a pure TA sample was also analyzed by the FTIR and presented in the figure. Table 3 presents the details of peaks and their assignments base on the FTIR spectra. The stretching and vibration modes of (–OH) group are present at 3423 cm^{-1} and 3434 cm^{-1}, respectively, corresponding to the chemically bound water molecules of the hydration product. Calcite, which is detected by XRD analysis, is also identified by the FTIR analysis.

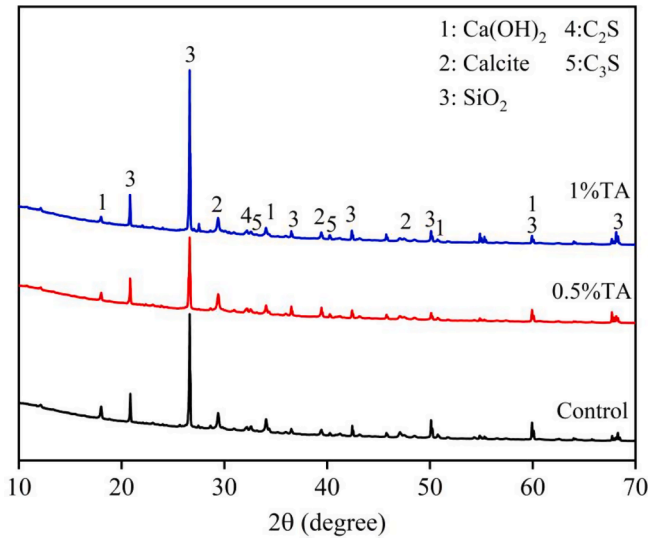

Fig. 5. XRD patterns of RCF samples.

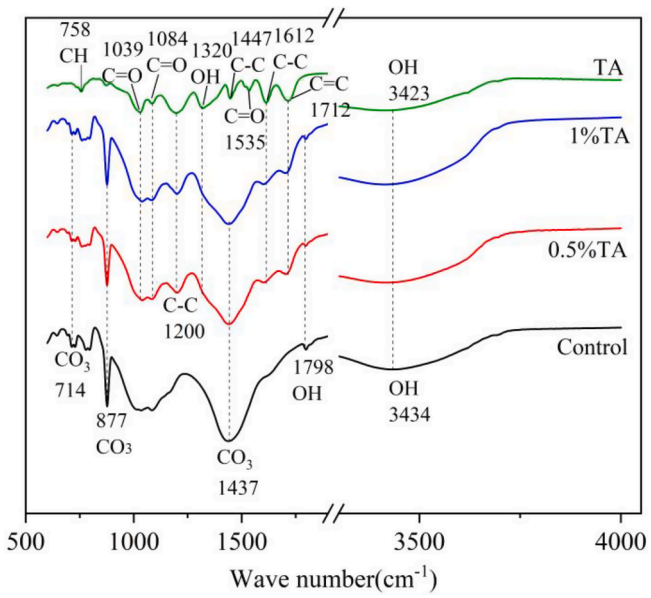

Fig. 6. FTIR spectra of TA, untreated and treated RCP.

Table 3
The detail of peaks base on the FTIR spectra (wave number: cm^{-1}).

RCP	0.5% TA	1% TA	TA	Assignment
3434	3430	3427	3423	(–OH) stretch of H-bond
1798	1797	1797	–	(–OH) stretch of CH
–	1705	1701	1712	(C=C) stretch of benzene ring
–	1601	1608	1612	(C–C) stretch and (C–H) deformation in plane of benzene ring
–	–	–	1535	(C=O) stretch of carboxylic acid
–	–	–	1447	C–C stretch of benzene ring
–	1319	1320	1320	(–OH) stretch in plane of benzene ring
–	1200	1200	1198	(C–C) stretch and (C–H) deformation in plane of benzene ring
–	1084	1085	1084	(C=O) stretch of carboxylic acid
–	1041	1039	1039	(C=O) stretch of carboxylic acid
877	876	876	–	CO_3 stretch of calcite
–	–	–	758	(C–H) torsion of benzene ring
714	711	711	–	CO_3 stretch of calcite

Calcite particles are present in all RCF samples, as indicated by the vibration of CO_3 bond at wave numbers 714 cm^{-1} and 877 cm^{-1}. These two peaks are weakened bythe TA treatment, indicating that some calcite in the RCF samples was consumed during the chemical reaction between the RCF and TA solution. The peak at 1798 cm^{-1} is caused by the (–OH) stretch of CH. The intensity of (–OH) stretch of CH is reduced by the TA treatment, suggesting that some CH was also consumed by chemical reaction with TA. This agrees with the results of XRD analysis shown in Fig. 5. The (C = C) stretch and (C–C) stretch in plane of benzene ring can be detected around 1612 cm^{-1} in the treated RCF samples, indicating that the benzene ring in TA can be left on the surface of the RCF particles. Meanwhile, the wave number at 1320 cm^{-1} refers to the (–OH) stretch in plane of benzene ring. This suggests that the formation of calcium-TA complex probably deposited on the surface of the RCF particles was induced by the coordination of polyphenol functional groups with the calcium ions through the chelation. This can also be confirmed by the blue shift of peaks of 1198 cm^{-1}, 1039 cm^{-1} [55].

3.1.3. SEM

Fig. 7 compares the microstructures of the untreated and treated RCF by the SEM analysis. The untreated RCF has a loose microstructure and rough surface with many pores as revealed by Fig. 7(a). TA treatment

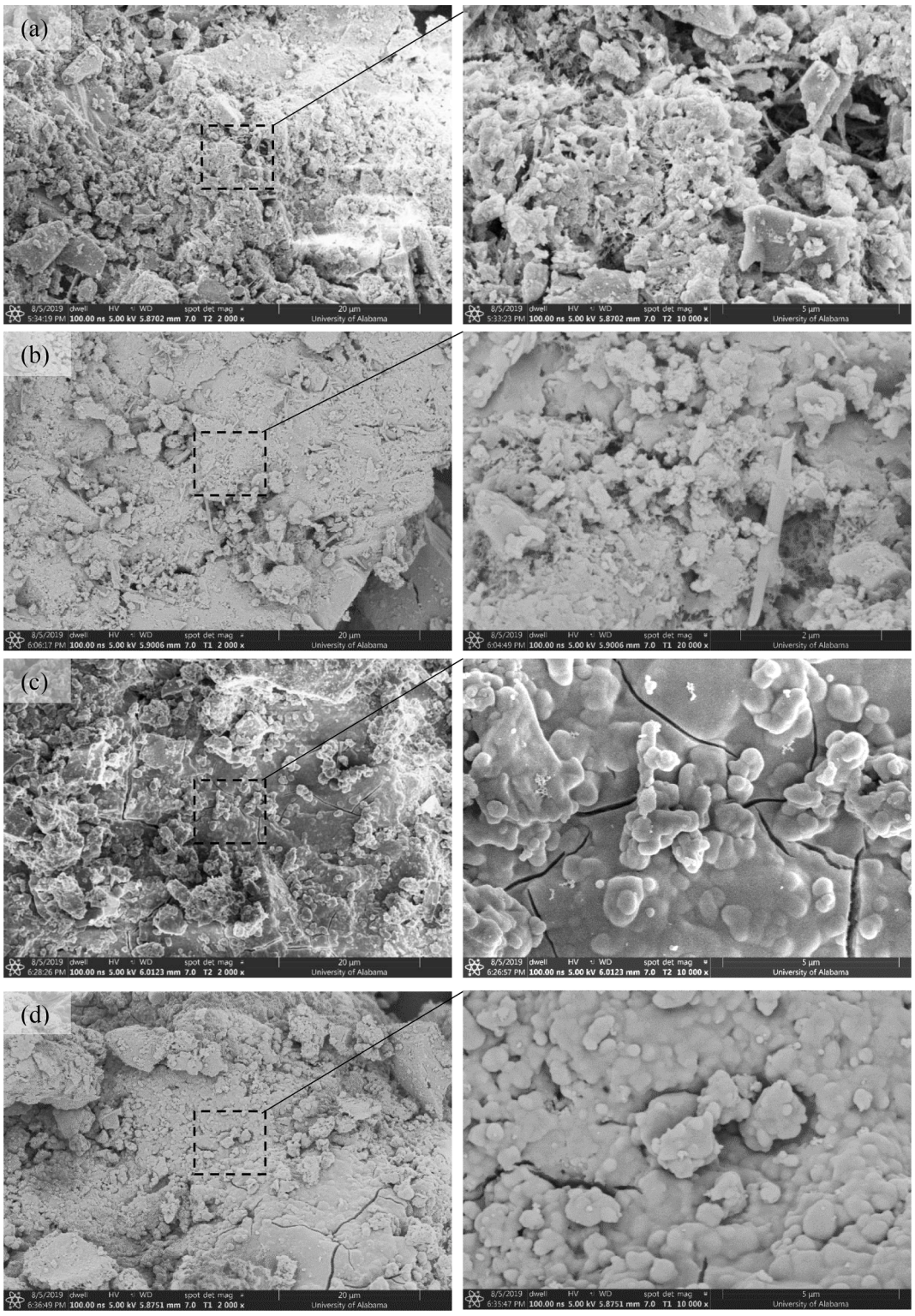

Fig. 7. SEM images of the RCF samples: (a) untreated; (b) treated with 0.1% TA; (c) treated with 0.5% TA; (d) treated with 1% TA.

clearly densifies the RCF samples, showed in Fig. 7(b), 7(c) and 7(d). This can mainly be attributed to two reasons: 1) Some of the loose material and very fine powders on the surface of the RCF particles were dissolved by the TA solutions; 2) Reaction products between TA and the RCF can fill the pores and crack of the RCF particles and deposit on the surface of the RCF particles. This can be seen very clearly on Fig. 7(c) and 7(d), in which the RCF samples were treated by 0.5% and 1% TA solutions, respectively. Large amount of submicron particles can be found on the surface of the treated RCF particle on these two samples. These particles are not visible on the sample treated with 0.1%TA solution because of the low concentration of TA used in the treatment. These particles should be calcium-TA complex of chelate products of TA and calcium ions, as indicated by the FTIR results shown in Fig. 6 and Table 3.

3.1.4. BET analysis

The effect of the proposed treatment on the pore structure of RCF is revealed by the BET analysis shown in Fig. 8. Both the pore size and the total porosity of the RCF have been significantly reduced by the treatment, agreeing with the SEM observation shown in Fig. 7. The only possible reason responsible for this reduction of porosity is that the reaction products between TA and RCF fill some of the pores. Fig. 8 shows that the reduction of the pore volume of the RCF specimen increases with the amount of TA used to treat the RCF. This is because more reaction products can be produced by using more TA. As a result, more pores can be filled by these products. With much lower porosity, the performance of the produced concrete/mortar should be drastically improved.

3.2. Properties of mortar with RCF

3.2.1. Hydration heat

Effect of the TA treatment on the hydration of the cement past is shown in Fig. 9. In this figure, the Control and RCF paste samples were made without and with the untreated RCF to replace 10% OPC, respectively. Those X% cement pastes were made with X% TA treated RCF to replace 10% OPC. Comparing the heat power curves of Control and RCF pastes suggests that replacing 10% cement with RCF accelerates the hydration of the resulted blended paste. This is not surprising since the RCF provides more seeding sites for the hydration of the cement. Compared with this paste with untreated RCF, all pastes with TA treated RCF produced higher thermal flow and more reaction heat at the first 6 h of the measurement, as revealed by Fig. 9. This suggests that reaction occurred between the residual TA and cement at this period. Nevertheless, residual TA also retards the hydration of the cement, as evidenced by the longer dormant period and reduced heat flow of the pastes with TA treated RCF, and this retarding effect increases with the concentration of TA. At lower concentrations (0.3% and 0.5%), this retarding effect quickly diminished. The accumulated hydration heats of the pastes surpassed that of the RCF paste, suggesting that TA treatment can promote the hydration of the cement. At higher concentrations (0.75% and 1.0%), much more severe retarding effect was induced by the residual TA and accumulated hydration heats of the pastes were lower than that of the RCF paste within the observation period. However, the gap between these values was narrowing with the hydration.

3.2.2. Compressive strength

Fig. 10 shows the effect of TA treatment on the compressive strength of the mortars at 3d, 7d and 28d. In this figure, X% refers to the mortar made with RCF treated with TA solution at X% in mass concentration. As a comparison, a group of mortar was prepared without using any RCF and TA, noted as "Control". Its compressive strengths at 3d, 7d, and 28d were measured as 19.97 MPa, 26.64 MPa and 39.17 MPa, respectively.

It can be seen that the compressive strength, especially the late age strength of the mortars with untreated RCF depends on the content of RCF used. At 5% of replacement, the produced mortar has a compressive strength close to the Control one. At higher replacement levels, the compressive strengths of the produced mortars at 28d are significantly lower than that of the Control one, indicating the lower reactivity of the RCF in comparison with the cement.

This drawback of using RCF as SCM can be mitigated by the proposed treatment. As shown in Fig. 10, the compressive strengths at 28d of the mortars with 10% RCF have been improved by 12.2%, 25.6%, 26.3%, 17.3%, and 13.1% after treating the RCF with 0.1%, 0.3%, 0.5%, 0.75%, and 1.0%, respectively. In this case, strength improvement first increases to a maximum value and then reduces with the concentration of TA. This suggests that there exists an optimal concentration of TA, at which the highest strength improvement at 28d can be reached by the treatment. Indeed, strength improvement is limited if too little TA is used, as revealed by the sample with RCF treated by 0.1% TA in this group. However, if too much TA is used, the retarding effect of residual TA becomes strong enough to reduce the compressive strength of the mortar in the measurement period, as indicated by the mortars with RCF treated with 0.75% and 1.0% TA. For this reason, the compressive strength of the sample with 1.0%TA treated RCF is lower than that of the sample with 0.75%TA. When appropriate amount of TA is used to treat the RCF, the compressive strength of the mortar with 10% RCF can surpass that of the one with 100% of cement, confirming the effectiveness of the proposed treatment.

Similar effect of TA on the compressive strength at 28d can be observed on the mortars made with 15% RCF. In this case, the compressive strengths at 28d of the mortar have been improved by 14.7%, 21.2%, 26.5%, 26.3%, and 18.2% after treating the RCF with 0.1%, 0.3%, 0.5%, 0.75%, and 1.0% TA solutions, respectively. In this case, the retarding effect of residual TA is not as strong as in the previous one, as evidenced by 26.3% strength improvement with 0.75% TA treatment. This is because more RCF was used in the sample, which reacted and consumed more TA. This trend can be seen even more clearly in mortars made with 20% RCF. In this case, higher compressive strength has been reached by using higher concentration of TA because less residual TA is present in the sample in comparison with the mortars with less RCF.

No significant strength improvement has been achieved for mortars with only too little (5%) or too much (20%) RCF, as indicated by Fig. 10. When only 5% RCF is used, the mortar strength is mainly controlled by the cement. Fig. 10 shows that the compressive strength of the mortar with 5% RCF even surpasses that of the Control sample. This can be

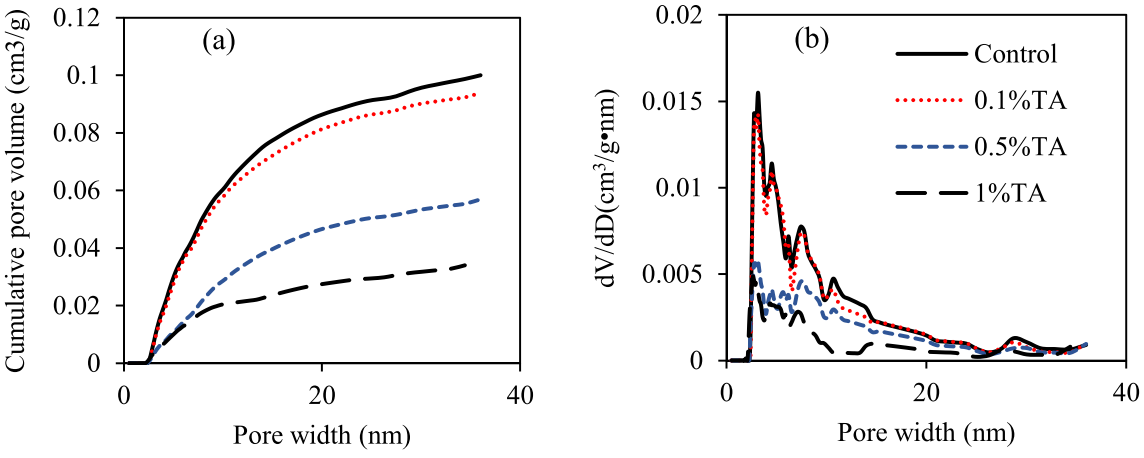

Fig. 8. The cumulative pore volume and pore volume distribution of the RCF samples: (a) cumulative pore volume; (b) pore volume distribution in the range of 0 nm-40 nm.

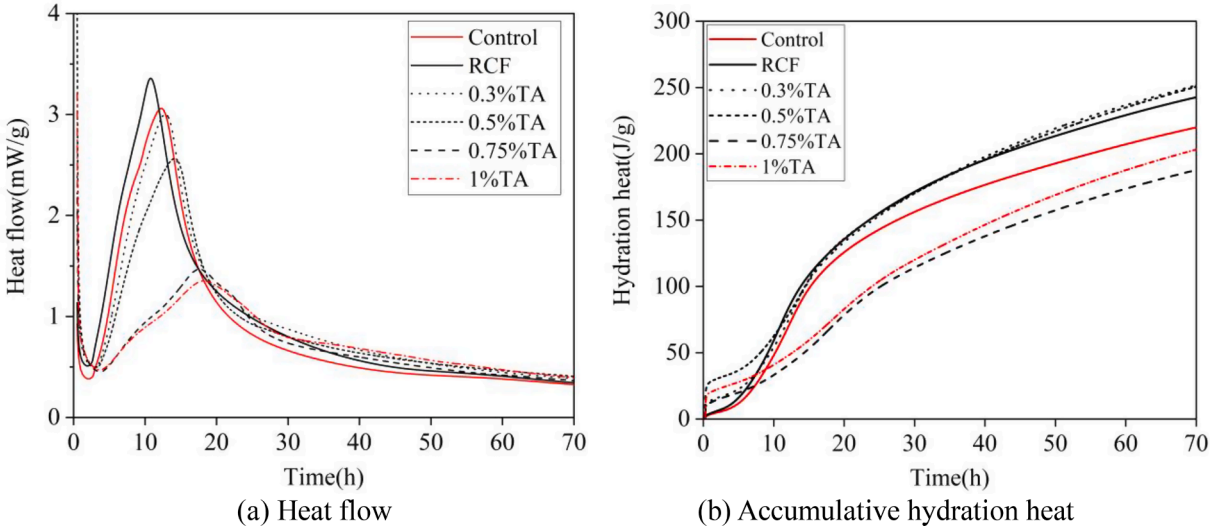

Fig. 9. Heat flow and hydration heat of cement blended with RCF.

attributed to the limited reactivity and seeding and filling effects of the RCF. However, RCF is highly porous material. If added in high content, the compressive strength of the mortar can be significantly reduced, which cannot be recovered by the proposed treatment, as revealed by the mortars with 20% RCF shown in Fig. 10.

3.2.3. *XRD analysis*

Fig. 11 compares XRD patterns of four cement pastes: RCF paste made with 10% cement replaced by the untreated RCF, and 0.3%TA, 0.5%TA, and 1%TA pastes made with 10% cement replaced by RCF treated with 0.3%TA, 0.5%TA, and 1%TA solutions, respectively. The CH, quartz (SiO_2), calcite ($CaCO_3$), dicalcium silicate (C_2S) and tricalcium silicate (C_3S) are the major crystalline compositions in those samples. The CH comes from the hydration of the new cement and residual CH in the RCF. The quartz comes from the natural fine aggregates (river sand) in the RCF. The calcite is induced by the carbonation of CH in the RCF and new cement paste. C_3S and C_2S come from the unhydrated cement, which are still detectable at 28d, suggesting that hydration of the cement is not completed. Compared with the paste with untreated RCF, no new characteristic peak was detected on the XRD spectra of all pastes with TA treated RCF. This suggests that TA treatment does not produce any new hydration product in the paste.

3.2.4. *Effect of TA treatment on the pore structures of the produced mortars*

To find out the reason causing the strength improvement observed in Fig. 10, MIP testing was carried out to examine the proposed treatment on the pore structure of the produced mortars at 28d, as presented in Fig. 12. Compared with the control sample made without any RCF, the RCF mortar made with 10% of cement replaced by untreated RCF has a significant higher porosity, as revealed by Fig. 12(a). This is expected since the untreated RCF is porous material and has much more pores larger than 100 nm, as shown in Fig. 12(b). These pores can be significantly reduced by the TA treatment, as shown in Fig. 12(b). This is because TA treatment not only densifies the RCF particles (Fig. 8), but also generates submicro particles which can fill many pores of the produced mortar. The filling effect of these particles also refines the capillary pores of the produced mortar in the range of 10 nm-100 nm. As shown in Fig. 12(b), peak size of the capillary pore of the RCF mortar is around 54 nm. This value is reduced to 43 nm after the RCF treated by 0.3%TA solution. As a result, the cumulative pore volume of this mortar sample (0.3%TA) is significantly lower than the RCF mortar, explaining why the compressive strength of mortar can be improved by using TA treated RCF. The porosity of the mortar is slightly increased by using 0.5%TA to treat the RCF, which can be attributed to the stronger retarding effect induced by more residual TA in the sample. This stronger retarding effect is also indicated by the slightly lower compressive strength at 28d of this mortar in comparison with the 0.3% TA mortar, as shown in Fig. 10(c).

The capillary pores can be classified as harmless (less than20 nm), almost harmless (20–100 nm), harmful (100–200 nm) and very harmful (greater than200 nm) [56]. Fig. 13 shows the pore volume in these four categories, in which the total volume fraction of harmful and very harmful pores and volume fraction of the almost harmless pores are also presented. By comparing the RCF mortar with Control sample, it is clear that replacing 10% Portland cement with RCF increases the volume fraction of the harmful and very harmful pores from the RCF mortar has a much higher volume fraction for 29.1% to 39.7%. This difference is induced by the porous nature of the RCF. Consequently, the compressive strength of the RCF mortar is much lower than that of Control mortar at 28d, as shown in Fig. 8. These harmful and very harmful pores brought into the mortar by the RCF can be drastically reduced by treating the RCF with TA, as revealed by their volume fraction in two mortars with TA treated RCF (0.3%TA and 0.5%TA mortars in Fig. 8). Therefore, the strengths of the produced mortars are much higher. Fig. 8 also shows that 0.5%TA sample has more harmful pores than the 0.3%TA sample, which can be attributed to the more severe retarding effect induced by using more TA to treat the RCF. Although the total volume of harmful and very harmful pores in the Control mortar is small that that of two mortars with TA treated RCF, the size of harmful pores in these two mortars are smaller than that of the Control sample, as shown in Fig. 12. Therefore, the compressive strength at 28d of these two mortars are higher than that of the Control one, as shown in Fig. 10.

3.2.5. *Nanoindentation analysis*

Fig. 14 compares the contour mappings and deconvolution of elastic modulus obtained from nanoindentation tests for the mortar made with 10% untreated RCF (RCF mortar) and another one made with 10% RCF treated with 0.5%TA solution (0.5%TA mortar). Two differences between these two mortars are revealed by the contour mapping of the elastic modulus shown in Fig. 14(a) and 14(c). First, there is much less low-modulus porous phases present in the 0.5%TA sample. This agrees with the MIP results presented in Figs. 12 and 13. Second, more high-modulus hydration products exist around the grey-color phases in the 0.5%TA mortar. The grey-color phases are small particles with elastic modulus higher than 60 GPa. They most likely are aggregates or unreacted cement particles. Previous study [57] shows that TA coated on the surface of the recycled cement mortar particle can capture calcium ions to induce local mineralization, leading to more and denser

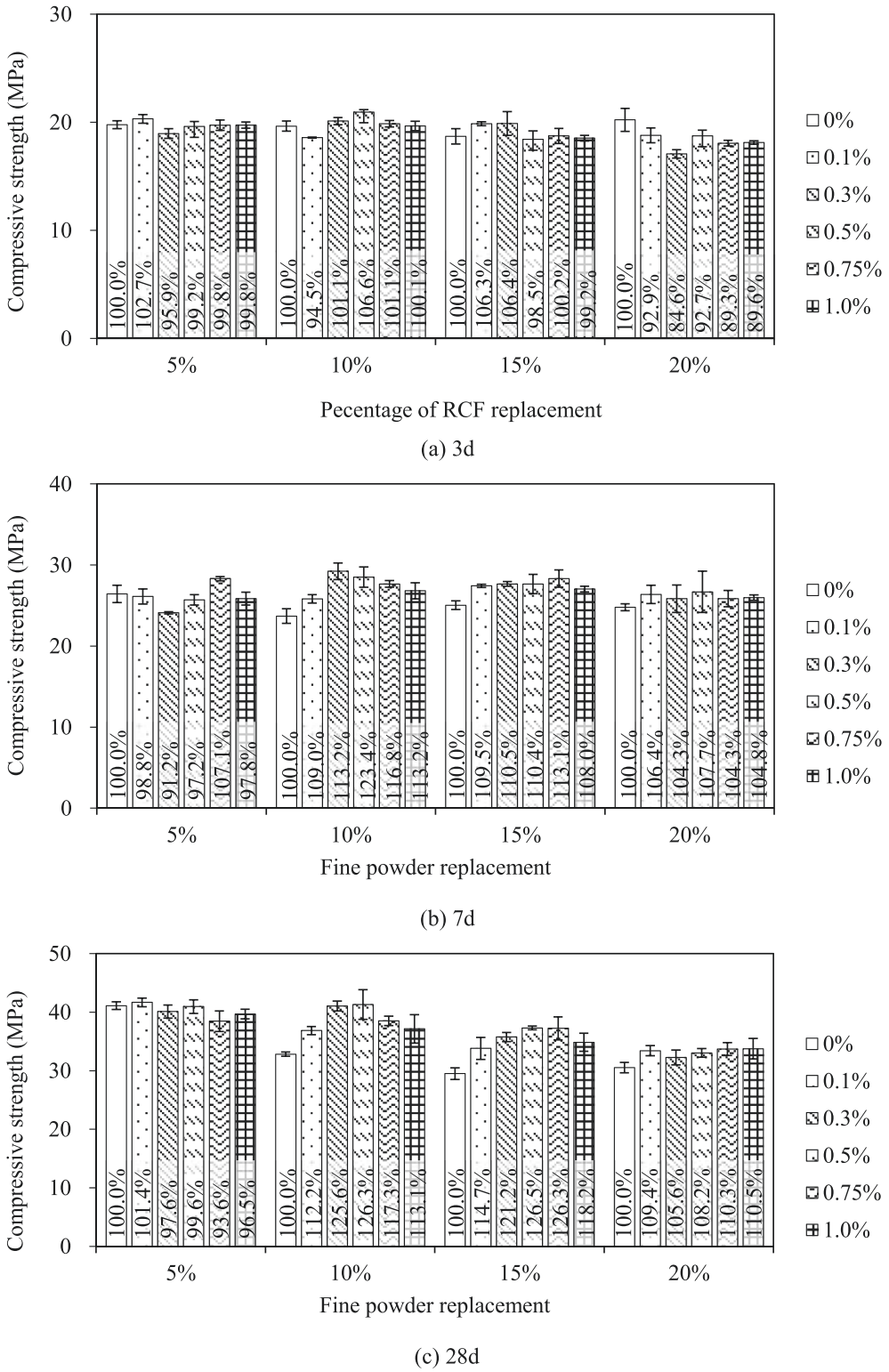

Fig. 10. Effect of TA treatment on the compressive strengths of the produced mortars.

hydration products around these hard particles, as shown in Fig. 14(c). As a result, the compressive strength of the mortar produced with TA treated RCF is much higher than the one made with the untreated RCF.

The densifying effect of TA treatment can be seen more clearly on the deconvolution of the modulus shown in Fig. 14(b) and (d). In these two figures, four hydration phases (LD, HD, UHD, and CH) and a low-modulus porous phase (PP) are used to fit the measured moduli and fitting parameters are also presented. These parameters are volume fraction of the phase (π), mean value (μ), and standard deviation (σ) of measured modulus of the phase. Two effects of the proposed treatment can be clearly seen from these two figures. First, TA treatment increases the mean elastic moduli of all five phases. Second, TA treatment reduces the PP from 38% to 35%, LD C-S-H from 39% to 33%, and increases the HD C-S-H from 19% to 27%. As a result, the overall average elastic modulus of all phases is increased by TA from 18.57GPa and 22.75GPa, indicating that TA treatment does densify the microstructure of the

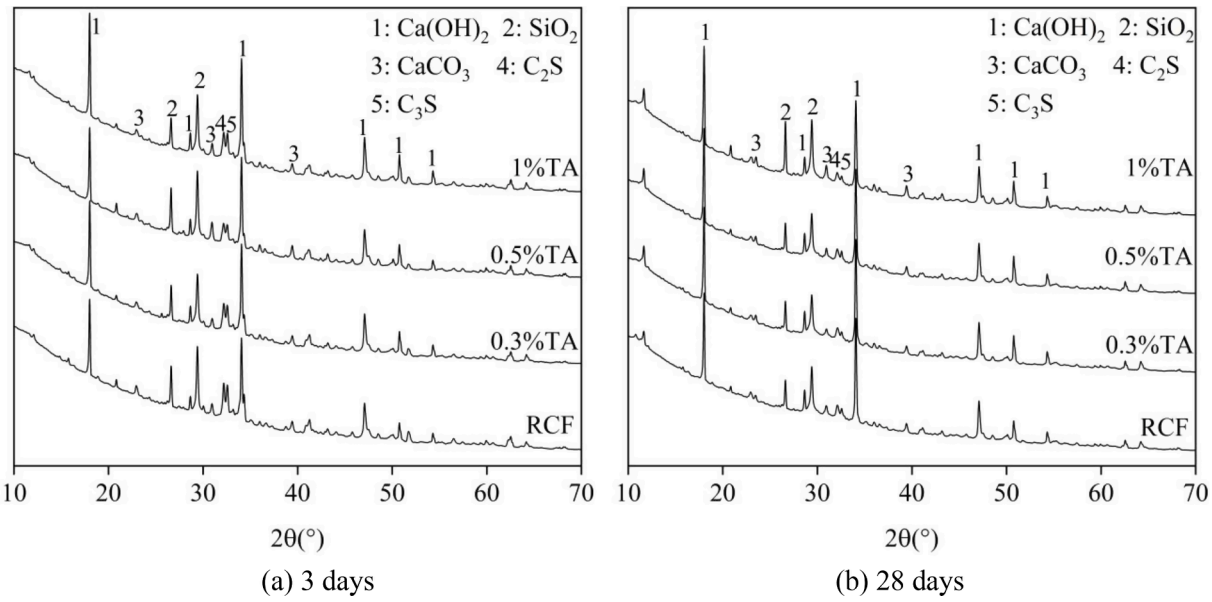

Fig. 11. XRD patterns of the cement paste with untreated and TA-treated RCF.

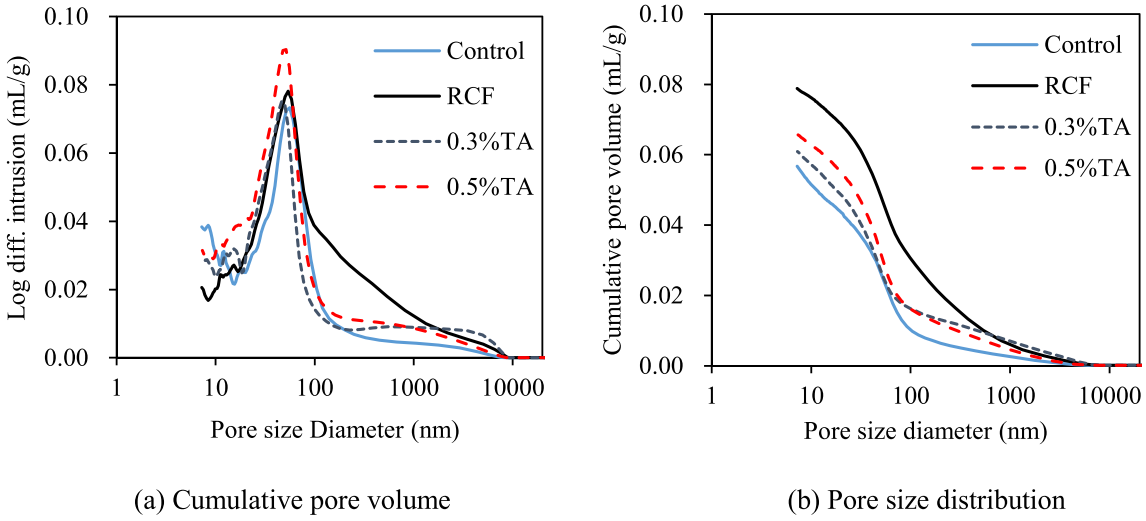

Fig. 12. Effect of TA treatment on the cumulative pore volume and pore size distribution of the produced mortar at 28d.

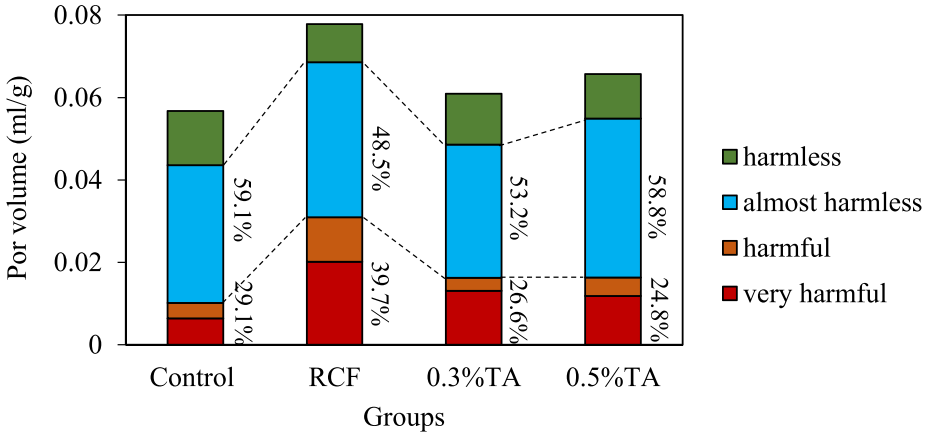

Fig. 13. Effect of TA treatment on the pore volume distribution of the produced mortars.

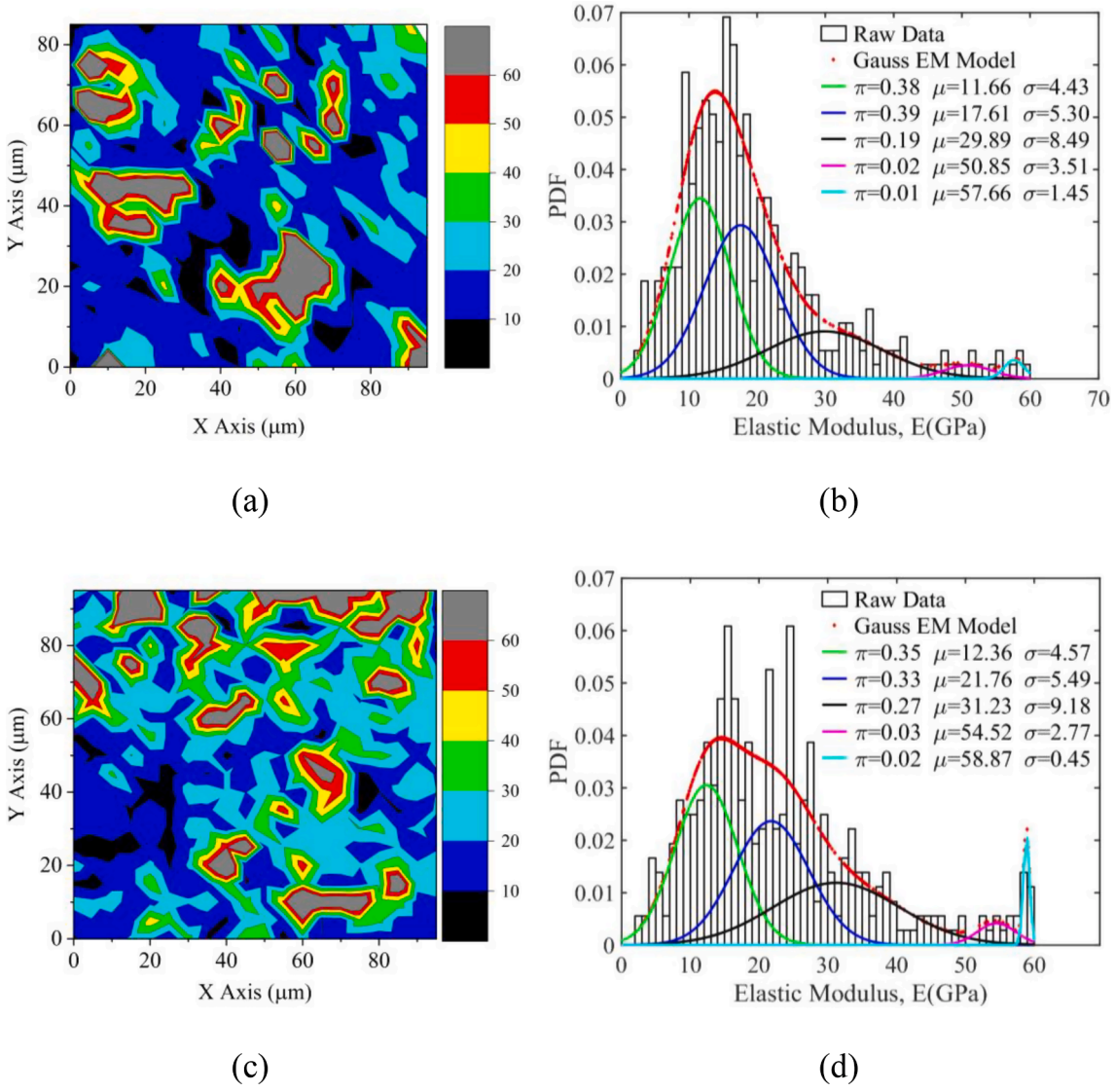

Fig. 14. Contour map of elastic modulus and deconvolution results of elastic modulus: (a) contour map of the elastic modulus of the RCF mortar; (b) the elastic modulus of the RCF mortar; (c) contour map of elastic modulus of the 0.5%TA mortar; (d) the elastic modulus of the 0.5%TA mortar.

hydration products.

The densifying effect of TA can be quantified using packing density, which is calculated based on elastic modulus shown in Fig. 14. Table 5 presents the mean packing densities and volume fractions of five phases detected in Fig. 14. It can be seen that the packing densities of all phases are improved after the TA treatment, and overall mean packing density of all phases is increased by 0.037, leading to higher compressive strength and better durability.

3.2.6. *Early-age cracking*

The effect of the proposed treatment on the early age cracking of the produced specimen is shown in Fig. 15. It is surprising to find that the specimen with untreated RCP exhibits a better ability to resist cracking than the control group, as indicated by its lower crack number and total crack area per unit area. This can be attributed to the high porosity of the RCF, which can absorb mixing water during mixing, leading to a reduction in drying shrinkage and enhancement in fracture energy [58]. As a result, all samples with RCF have much less early-age cracks than the mortar with 100% OPC. Those early age cracks can be further reduced by the proposed treatment. As shown in Fig. 15, the crack numbers, crack areas per unit area, and crack area per crack all experience significantly reduction, and the reduction increases with the increase of the TA content used to treat the RCF. This reduction on early age cracking induced by TA can be attributed to two mechanisms: 1) TA can reduce the heat release and hydration heat at the early age, as show in Fig. 9; 2) TA is hydrophilic which can reduce the evaporation of water from the sample. Therefore, the proposed treatment with TA can significantly suppress the cracking in the early age concrete, leading to

Table 5
Packing density of the hydration phases.

Groups	PP		LD		HD		UHD		CH		Overall
	Volume	Mean	Volume	Mean	Volume	Mean	Volume	Mean	Volume	Mean	
RCF	0.38	0.60	0.39	0.65	0.19	0.75	0.02	0.92	0.01	0.98	0.651
0.5%TA	0.35	0.60	0.33	0.68	0.27	0.76	0.03	0.95	0.02	0.99	0.688

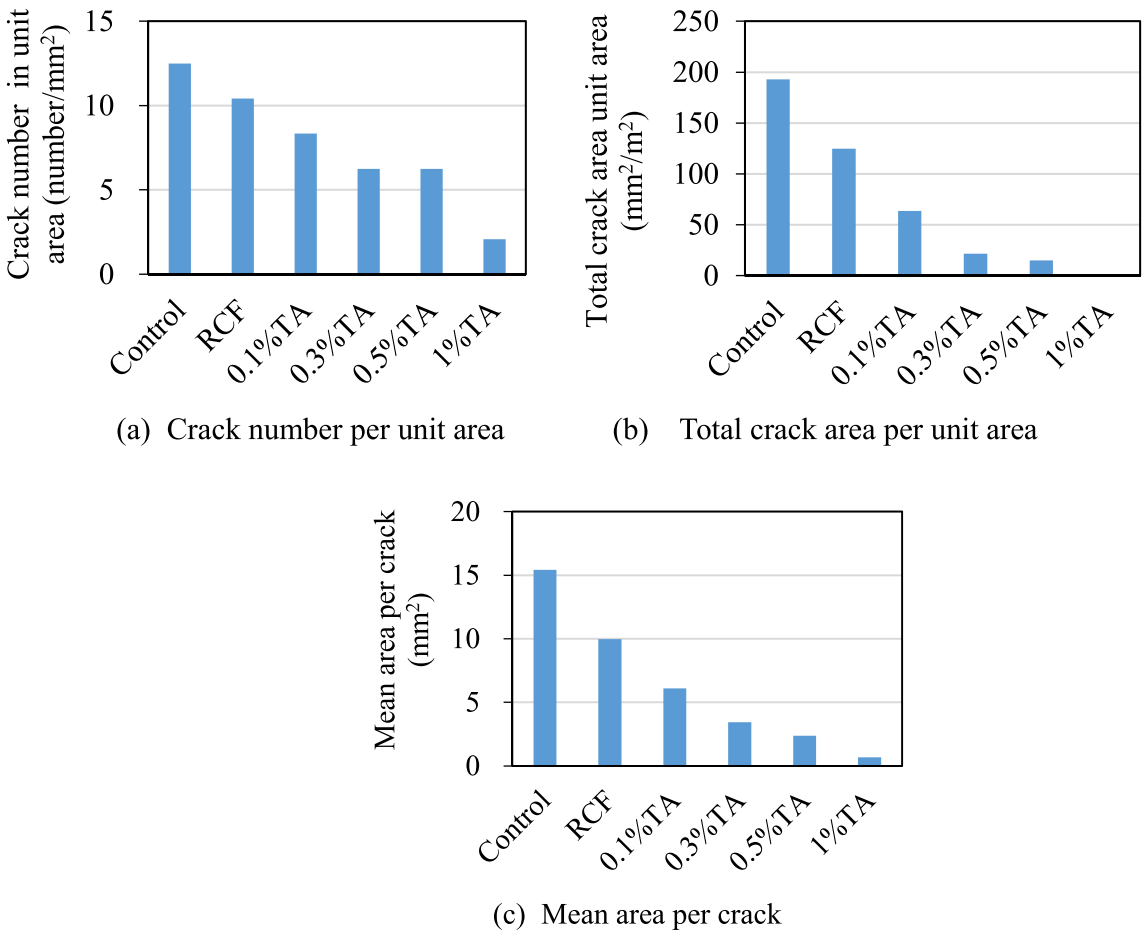

Fig. 15. Effect of TA treatment on the early-age cracking parameters of produced mortar.

much higher long-term durability of the produced concrete.

3.2.7. Effect of the TA treatment on corrosion of the steel reinforcement

Accelerated corrosion testing results are shown in Fig. 16, in which the corrosion current is plotted again time. When the through crack(s) is generated, resistance between the positive and the negative poles is drastically decreased, resulting in a sudden increase in the current. Therefore, the time at which the current starts to increase sharply is reported as the corrosion time of the specimen, which is labeled in Fig. 16 (a) for each specimen. Fig. 16(b) compares the corrosion times of mortars with untreated and TA-treated RCF. Compared with the Control mortar without any RCF, the mortar with 10% cement replaced by untreated RCF has a shorter corrosion time, suggesting that this mortar has a lower corrosion resistance. This is not surprising since the untreated RCF is highly porous.

No significant improvement on the corrosion time can be achieved by treating the RCF using 0.1%TA, indicating low concentration of TA is not sufficient to protect the reinforcement. Increasing the concentration of TA to 0.3% and above, the corrosion time of the produced mortar can be significantly increased. For example, treating the RCF with 0.3%TA increases the corrosion time of the mortar from 86 h to 133 h. Clearly, the lower porosity (Fig. 12), denser hydration products (Fig. 14) and higher mechanical strength (Fig. 10) induced by TA treatment all contribute to the much-improved corrosion resistance of the mortars.

Moreover, Fig. 16(b) shows that the corrosion times of 0.3%TA, 0.5% TA, and 1%TA mortars all surpass that of the Control one, indicating that TA can be used to enhance the corrosion resistance of cement mortar. Indeed, existing study shows that TA acts as a cathodic-type corrosion inhibitor, retarding the cathodic process of the corrosion reactions by forming ferric tannates on the mild steel surface [59]. TA can react with the initial rust c-FeOOH easily [60] to form TA-iron complex, which will be oxidized to ferric tannate. Ferric tennate is very stable and much dense than the rust, acting as a physical barrier to protect the reinforcing steel in concrete from corrosion.

4. Conclusion

This study proposes an eco-friendly method to enhance the performance of cement mortar made with RCF to partially replace OPC through a simple two-step mixing process. A naturally occurring compound, TA is used in the first mixing step to react with RCF. The products of this reaction not only fill the pores in the RCF, but also deposit on the surface of RCF particles as submicron particles. These particles can seed the hydration of cement and fill the pores of the paste, leading to denser microstructure. This has been confirmed by MIP testing and nano-indentation testing, which demonstrate that TA treatment can significantly reduce the porosity and enhance the elastic modulus and packing density of the hydration products. As a result, the compressive strength at 28d of the mortar made with RCF as SCM can be improved over 26% by the proposed methods. More importantly, the durability of the produced mortar can be drastically improved by the proposed treatment too. For example, the early-age cracking of the mortar can be significantly reduced by the proposed treatment. The corrosion time is enhanced by the proposed method over 55%. Compared with existing methods which may require strong acid/alkaline or energy intense process such as calcination or carbonation, the proposed method only uses a ubiquitous, non-toxic, renewable, and low-cost biomolecule to treat RCF. This method does not require any extra equipment and

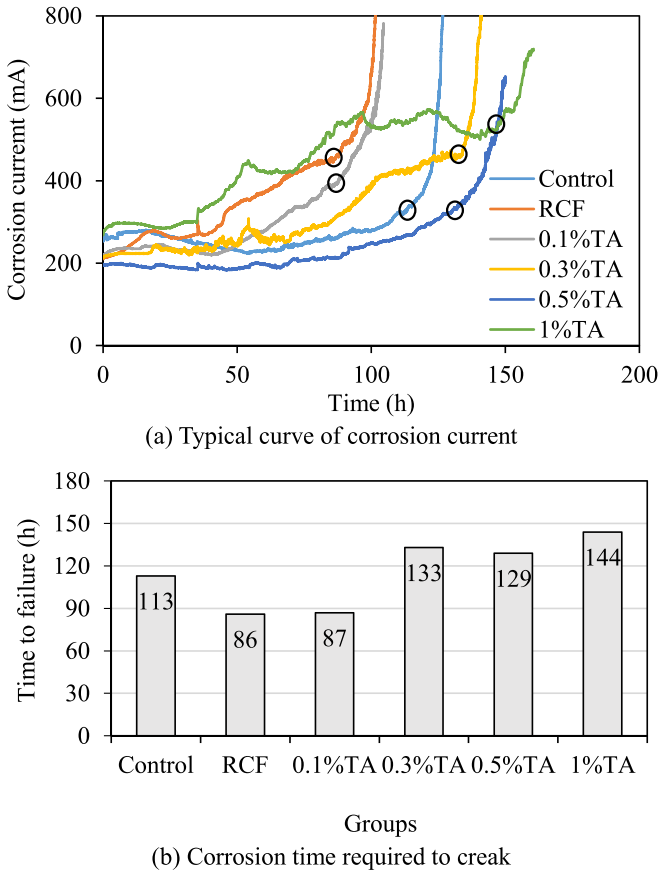

Fig. 16. Corrosion current curve and time of mortar specimen.

produces zero waste. In addition, this study introduces a new class of eco-friendly biomolecule to enhance the performance of RCFs so that they can be used to replace OPC. It can be envisioned that Some TA-rich natural plant extracts, such as tea-leaf, may also work to treat RCF and other C&D wastes. More research will be carried out in this area in the future.

CRediT authorship contribution statement

Liang Wang: Methodology, Investigation, Writing – original draft, Visualization. **Jialai Wang:** Conceptualization, Writing – review & editing, Funding acquisition, Supervision. **Hao Wang:** Investigation. **Yi Fang:** Investigation. **Wenfeng Shen:** Investigation. **Peiyuan Chen:** Investigation. **Ying Xu:** Investigation, Supervision.

Declaration of Competing Interest

The authors declare that they have no known competing financial interests or personal relationships that could have appeared to influence the work reported in this paper.

Acknowledgements

This work was supported by the National Science Foundation –United States (CMMI 1761672), Alabama Transportation Institute, Natural Science Foundation of China (NO. 52108187 and 52008003), China Postdoctoral Science Foundation (NO. 2020M681988), Natural Science Foundation of Universities in Anhui Province (KJ2019A0129), Key Research and Development Project of Anhui Province (201904a07020081) and Anhui Provincial Natural Science Foundation (2008085QE244).

References

[1] M. Menegaki, D. Damigos, A review on current situation and challenges of construction and demolition waste management, Curr. Opin. Green Sustain. Chem. 13 (2018) 8–15, https://doi.org/10.1016/j.cogsc.2018.02.010.
[2] H. Dahlbo, J. Bachér, K. Lähtinen, T. Jouttijärvi, P. Suoheimo, T. Mattila, S. Sironen, T. Myllymaa, K. Saramäki, Construction and demolition waste management – a holistic evaluation of environmental performance, J. Clean. Prod. 107 (2015) 333–341, https://doi.org/10.1016/j.jclepro.2015.02.073.
[3] Y. Kim, Quality properties of self-consolidating concrete mixed with waste concrete powder, Constr. Build. Mater. 135 (2017) 177–185, https://doi.org/10.1016/j.conbuildmat.2016.12.174.
[4] L. Li, D. Xuan, A.O. Sojobi, S. Liu, S.H. Chu, C.S. Poon, Development of nano-silica treatment methods to enhance recycled aggregate concrete, Cem. Concr. Compos. 118 (2021), 103963, https://doi.org/10.1016/j.cemconcomp.2021.103963.
[5] W.M. Shaban, K. Elbaz, J. Yang, B.S. Thomas, X. Shen, LiHui Li, Y. Du, J. Xie, L. Li, Effect of pozzolan slurries on recycled aggregate concrete: Mechanical and durability performance, Constr. Build. Mater. 276 (2021) 121940, https://doi.org/10.1016/j.conbuildmat.2020.121940.
[6] X. Chen, J. Zheng, Influence of recycled Powder on Hydration Characteristics of Cement Paste (In Chinese), Bull. Chinese Ceram. Soc. 8 (2016) 2530–2536,2542.
[7] J. Xiao, Z. Ma, T. Sui, A. Akbarnezhad, Z. Duan, Mechanical properties of concrete mixed with recycled powder produced from construction and demolition waste, J. Clean. Prod. 188 (2018) 720–731, https://doi.org/10.1016/j.jclepro.2018.03.277.
[8] Z. Duan, S. Hou, J. Xiao, B. Li, Study on the essential properties of recycled powders from construction and demolition waste, J. Clean. Prod. 253 (2020), 119865, https://doi.org/10.1016/j.jclepro.2019.119865.
[9] C. Zhou, H. Ji, L. Zhao, Application and Research Progress of Recycled Micro-powders in Cement-Based Materials (in Chinese), Bull. Chinese Ceram. Soc. 38 (2019) 2456–2463.
[10] Z. Prošek, J. Trejbal, V. Nežerka, V. Goliáš, M. Faltus, P. Tesárek, Recovery of residual anhydrous clinker in finely ground recycled concrete, Resour. Recycl. 155 (2020), 104640, https://doi.org/10.1016/j.resconrec.2019.104640.
[11] J. Peng, Experimental study on the activity of recycled fine powder composite cementitious material (master dissertation), Guangzhou University, 2019.
[12] H. Salahuddin, L. Ali, A. Nawaz, S. Safdar, Effect of recycled fine aggregates on performance of Reactive Powder Concrete, Constr. Build. Mater. 243 (2020), 118223, https://doi.org/10.1016/j.conbuildmat.2020.118223.
[13] K.Q. Yu, W. Zhu, Y. Ding, Z. Lu, J. Yu, J. Xiao, Micro-structural and mechanical properties of ultra-high performance engineered cementitious composites (UHP-ECC) incorporation of recycled fine powder (RFP), Cem. Concr. Res. 124 (2019), 105813, https://doi.org/10.1016/j.cemconres.2019.105813.
[14] Z. Duan, S. Hou, J. Xiao, A. Singh, Rheological properties of mortar containing recycled powders from construction and demolition wastes, Constr. Build. Mater. 237 (2020), 117622, https://doi.org/10.1016/j.conbuildmat.2019.117622.
[15] Z. Duan, A. Singh, J. Xiao, S. Hou, Combined use of recycled powder and recycled coarse aggregate derived from construction and demolition waste in self-compacting concrete, Constr. Build. Mater. 254 (2020), 119323, https://doi.org/10.1016/j.conbuildmat.2020.119323.
[16] Y. Sui, C. Ou, S. Liu, J. Zhang, Q. Tian, Study on properties of waste concrete powder by thermal treatment and application in mortar, Appl. Sci. 10 (2020) 998, https://doi.org/10.3390/app10030998.
[17] L. Zhao, Study on basic properties and application of recycled fine powder from construction waste (master dissertation), Beijing University of Civil Engineering and Architecture (2019).
[18] Q. Liu, T. Tong, S. Liu, D. Yang, Q. Yu, Investigation of using hybrid recycled powder from demolished concrete solids and clay bricks as a pozzolanic supplement for cement, Constr. Build. Mater. 73 (2014) 754–763, https://doi.org/10.1016/j.conbuildmat.2014.09.066.
[19] S. Li, J. Gao, Q. Li, X. Zhao, Investigation of using recycled powder from the preparation of recycled aggregate as a supplementary cementitious material, Constr. Build. Mater. 267 (2021), 120976, https://doi.org/10.1016/j.conbuildmat.2020.120976.
[20] Z. Prošek, V. Nežerka, R. Hlůžek, J. Trejbal, P. Tesárek, G. Karra'a, Role of lime, fly ash, and slag in cement pastes containing recycled concrete fines, Constr. Build. Mater. 201 (2019) 702–714. 10.1016/j.conbuildmat.2018.12.227.
[21] B. Lu, C. Shi, J. Zhang, J. Wang, Effects of carbonated hardened cement paste powder on hydration and microstructure of Portland cement, Constr. Build. Mater. 186 (2018) 699–708, https://doi.org/10.1016/j.conbuildmat.2018.07.159.
[22] M. Zajac, J. Skocek, P. Durdzinski, F. Bullerjahn, J. Skibsted, M., Ben Haha, Effect of carbonated cement paste on composite cement hydration and performance, Cem. Concr. Res. 134 (2020), 106090, https://doi.org/10.1016/j.cemconres.2020.106090.
[23] P. Shen, Y. Sun, S. Liu, Y. Jiang, H. Zheng, D. Xuan, J. Lu, C.S. Poon, Synthesis of amorphous nano-silica from recycled concrete fines by two-step wet carbonation, Cem. Concr. Res. 147 (2021), 106526, https://doi.org/10.1016/j.cemconres.2021.106526.
[24] A.E. Hagerman, K.M. Riedl, G.A. Jones, K.N. Sovik, N.T. Ritchard, P.W. Hartzfeld, T.L. Riechel, High Molecular Weight Plant Polyphenolics (Tannins) as Biological Antioxidants, J. Agric. Food Chem. 46 (5) (1998) 1887–1892, https://doi.org/10.1021/jf970975b.
[25] X. Fei, W. Wei, F. Zhao, Y.e. Zhu, J. Luo, M. Chen, X. Liu, Efficient Toughening of Epoxy-Anhydride Thermosets with a Biobased Tannic Acid Derivative, ACS Sustain. Chem. Eng. 5 (1) (2017) 596–603, https://doi.org/10.1021/acssuschemeng.6b0196710.1021/acssuschemeng.6b01967.s001.

[26] J. Liu, H. Chen, Z. Xu, S. Zheng, M. Xue, Adsorption of tannic acid from aqueous solution by aminopropyl functionalized SBA-15, Desalin. Water Treat. 56 (2) (2015) 475–484, https://doi.org/10.1080/19443994.2014.940394.
[27] A. Arbenz, L. Avérous, Chemical modification of tannins to elaborate aromatic biobased macromolecular architectures, Green Chem. 17 (5) (2015) 2626–2646, https://doi.org/10.1039/C5GC00282F.
[28] Q. Wei, R. Haag, Universal polymer coatings and their representative biomedical applications, Mater. Horizons. 2 (6) (2015) 567–577.
[29] D. Lin, B. Xing, Tannic Acid Adsorption and Its Role for Stabilizing Carbon Nanotube Suspensions, Environ. Sci. Technol. 42 (16) (2008) 5917–5923, https://doi.org/10.1021/es800329c.
[30] S.C. Tam, J.G. McColl, Aluminum- and Calcium-Binding Affinities of Some Organic Ligands in Acidic Conditions, J. Environ. Qual. 19 (3) (1990) 514–520, https://doi.org/10.2134/jeq1990.00472425001900030027x.
[31] D.X. Oh, E. Prajatelistia, S.-W. Ju, H. Jeong Kim, S.-J. Baek, H. Joon Cha, S. Ho Jun, J.-S. Ahn, D. Soo Hwang, A rapid, efficient and facile solution for dental hypersensitivity: The tannin–iron complex, Sci. Rep. 5 (2015) 10884. 10.1038/srep10884.
[32] H. Ejima, J.J. Richardson, K. Liang, J.P. Best, M.P. van Koeverden, G.K. Such, J. Cui, F. Caruso, One-Step Assembly of Coordination Complexes for Versatile Film and Particle Engineering, Science 341 (6142) (2013) 154–157.
[33] J. Guo, Y. Ping, H. Ejima, K. Alt, M. Meissner, J.J. Richardson, Y. Yan, K. Peter, D. vonElverfeldt, C.E. Hagemeyer, F. Caruso, Engineering Multifunctional Capsules through the Assembly of Metal-Phenolic Networks, Angew. Chemie Int. Ed. 53 (22) (2014) 5546–5551, https://doi.org/10.1002/anie.201311136.
[34] W. Zhang, Z.Y. Yang, R.C. Tang, J.P. Guan, Y.F. Qiao, Application of tannic acid and ferrous ion complex as eco-friendly flame retardant and antibacterial agents for silk, J. Clean. Prod. 250 (2020), 119545, https://doi.org/10.1016/j.jclepro.2019.119545.
[35] Z. Zhang, Y. Sun, Y. Zheng, W. He, Y. Yang, Y. Xie, Z. Feng, K. Qiao, A biocompatible bacterial cellulose/tannic acid composite with antibacterial and anti-biofilm activities for biomedical applications, Mater. Sci. Eng. C. 106 (2020), 110249, https://doi.org/10.1016/j.msec.2019.110249.
[36] M. Dierendonck, K. Fierens, R. De Rycke, L. Lybaert, S. Maji, Z. Zhang, Q. Zhang, R. Hoogenboom, B.N. Lambrecht, J. Grooten, J.P. Remon, S. De Koker, B.G. De Geest, Nanoporous Hydrogen Bonded Polymeric Microparticles: Facile and Economic Production of Cross Presentation Promoting Vaccine Carriers, Adv. Funct. Mater. 24 (2014) 4634–4644, https://doi.org/10.1002/adfm.201400763.
[37] C. Yang, H. Wu, X. Yang, J. Shi, X. Wang, S. Zhang, Z. Jiang, Coordination-Enabled One-Step Assembly of Ultrathin, Hybrid Microcapsules with Weak pH-Response, ACS Appl. Mater. Interfaces. 7 (17) (2015) 9178–9184, https://doi.org/10.1021/acsami.5b01463.
[38] J. Chen, L. Qiu, Q. Li, J. Ai, H. Liu, Q. Chen, Rapid hemostasis accompanied by antibacterial action of calcium crosslinking tannic acid-coated mesoporous silica/silver Janus nanoparticles, Mater. Sci. Eng. C. 123 (2021), 111958, https://doi.org/10.1016/j.msec.2021.111958.
[39] P. Kord Forooshani, B.P. Lee, Recent approaches in designing bioadhesive materials inspired by mussel adhesive protein, J. Polym. Sci. Part A, Polym. Chem. 55 (1) (2017) 9–33, https://doi.org/10.1002/pola.28368.
[40] C.Y. Tang, P. Yu, L.S. Tang, Q.Y. Wang, R.Y. Bao, Z.Y. Liu, M.B. Yang, W. Yang, Ecotoxicology and Environmental Safety Tannic acid functionalized graphene hydrogel for organic dye adsorption, Ecotoxicol. Environ. Saf. 165 (2018) 299–306, https://doi.org/10.1016/j.ecoenv.2018.09.009.
[41] D.Y. Tang, J. Lyu, W. He, J. Chen, G. Yang, P.J. Liu, Q.L. Yan, Metastable intermixed Core-shell Al@M(IO3)x nanocomposites with improved combustion efficiency by using tannic acid as a functional interfacial layer, Chem. Eng. J. 384 (2020), 123369, https://doi.org/10.1016/j.cej.2019.123369.
[42] ASTM C109, Standard Test Method for Compressive Strength of Hydraulic Cement Mortars, ASTM International, West Conshohocken, PA, USA, 2016.
[43] ASTM C1702-17, Standard Test Method for Measurement of Heat of Hydration of Hydraulic Cementitious Materials Using Isothermal Conduction Calorimetry, ASTM International, West Conshohocken, PA, 2017.
[44] P. Monda, Nanomechanical properties of cementitious materials, Northwestern University, 2018.
[45] W.C. Oliver, G.M. Pharr, Measurement of hardness and elastic modulus by instrumented indentation: Advances in understanding and refinements to methodology, J. Mater. Res. 19 (2004) 3–20, https://doi.org/10.1557/jmr.2004.19.1.3.
[46] W. Zhu, J.J. Hughes, N. Bicanic, C.J. Pearce, Nanoindentation mapping of mechanical properties of cement paste and natural rocks, Mater. Charact. 58 (11-12) (2007) 1189–1198, https://doi.org/10.1016/j.matchar.2007.05.018.
[47] R.J.M. Pellenq, A. Kushima, R. Shahsavari, K.J. Van Vliet, M.J. Buehler, S. Yip, F. J. Ulm, A realistic molecular model of cement hydrates, Proc. Natl. Acad. Sci. 106 (38) (2009) 16102–16107, https://doi.org/10.1073/pnas.0902180106.
[48] P.D. Tennis, H.M. Jennings, A model for two types of calcium silicate hydrate in the microstructure of Portland cement pastes, Cem. Concr. Res. 30 (6) (2000) 855–863, https://doi.org/10.1016/S0008-8846(00)00257-X.
[49] H.C. Pedrosa, O.M. Reales, V.D. Reis, M. das D. Paiva, E.M.R. Fairbairn,, Hydration of Portland cement accelerated by C-S-H seeds at different temperatures, Cem. Concr. Res. 129 (2020), 105978, https://doi.org/10.1016/j.cemconres.2020.105978.
[50] M. Vandamme, F. Ulm, Nanoindentation investigation of creep properties of calcium silicate hydrates, Cem. Concr. Res. 52 (2013) 38–52, https://doi.org/10.1016/j.cemconres.2013.05.006.
[51] E. Lee, S. Park, Y. Kim, Drying shrinkage cracking of concrete using dune sand and crushed sand, Constr. Build. Mater. 126 (2016) 517–526, https://doi.org/10.1016/j.conbuildmat.2016.08.141.
[52] A. Leemann, P. Nygaard, P. Lura, Impact of admixtures on the plastic shrinkage cracking of self-compacting concrete, Cem. Concr. Compos. 46 (2014) 1–7, https://doi.org/10.1016/j.cemconcomp.2013.11.002.
[53] GB50082, Standard for Test Methods of Long-term Performance and Durability of Ordinary Concrete, China Architecture and Building Press, Beijing, 2009.
[54] E. Güneyisi, T. Özturan, M. Gesoğlu, A study on reinforcement corrosion and related properties of plain and blended cement concretes under different curing conditions, Cem. Concr. Compos. 27 (4) (2005) 449–461, https://doi.org/10.1016/j.cemconcomp.2004.05.006.
[55] S. Kim, A. Pasc, Advances in Multifunctional Surface Coating Using Metal-Phenolic Networks, Bull. Korean Chem. Soc. 38 (5) (2017) 519–520, https://doi.org/10.1002/bkcs.11123.
[56] Z. Wu, H. Lian, High Performance Concrete, China Railway Press, Beijing, China, 1999.
[57] L. Wang, J. Wang, X. Qian, Y. Fang, P. Chen, A. Tuinukuafe, Tea stain-inspired treatment for fine recycled concrete aggregates, Constr. Build. Mater. 262 (2020), 120027, https://doi.org/10.1016/j.conbuildmat.2020.120027.
[58] V. Nežerka, P. Havlásek, J. Trejbal, Mitigating inclusion-induced shrinkage cracking in cementitious composites by incorporating recycled concrete fines, Constr. Build. Mater. 248 (2020), 118673, https://doi.org/10.1016/j.conbuildmat.2020.118673.
[59] B. Qian, B. Hou, M. Zheng, The inhibition effect of tannic acid on mild steel corrosion in seawater wet/dry cyclic conditions, Corros. Sci. 72 (2013) 1–9, https://doi.org/10.1016/j.corsci.2013.01.040.
[60] S. Nasrazadani, The application of infrared spectroscopy to a study of phosphoric and tannic acids interactions with magnetite (Fe3O4), goethite (α-FEOOH) and lepidocrocite (γ-FeOOH), Corros. Sci. 39 (10-11) (1997) 1845–1859, https://doi.org/10.1016/S0010-938X(97)00060-7.